Published in final edited form as:
Nat Med. ; 17(9): 1109–1115. doi:10.1038/nm.2416.

Postpartum mammary gland involution drives DCIS progression through collagen and COX-2

Traci R Lyons[1,*], **Jenean O'Brien**[1,2,*], **Virginia Borges**[1,3], **Matthew W Conklin**[4,5], **Patricia J Keely**[4,5], **Kevin W Eliceiri**[5], **Andriy Marusyk**[6], **Aik-Choon Tan**[1,3], and **Pepper Schedin**[1,2,3,7]

[1]Department of Medicine, Division of Medical Oncology, University of Colorado Denver, MS8117, RC-1S, 8401K, 12801 E 17th Ave, Aurora, CO, USA 80045

[2]Program in Cancer Biology, University of Colorado Denver, MS8104, RC-1S, 5117, 12801 E 17th Ave, Aurora, CO, USA 80045

[3]University of Colorado Cancer Center, Bldg 500, Suite 6004C, 13001 E 17th Place, Aurora, CO, USA 0045

[4]Department of Cell and Regenerative Biology and UW Carbone Cancer Center, 1525 Linden Drive, University of Wisconsin, Madison, WI, USA 53706

[5]Laboratory of Cell and Molecular Biology, Laboratory for Optical and Computational Instrumentation, University of Wisconsin, Madison, WI, USA 53706

[6]Department of Medical Oncology, Dana-Farber Cancer Institute, Department of Medicine, Harvard Medical School, Boston, MA, USA 02115

[7]AMC Cancer Research Center, 3401 Quebec Street, Suite 3200, Denver, CO 80207

Abstract

Prognosis of young women's breast cancer is influenced by reproductive history. Women diagnosed within five years postpartum have worse prognosis than nulliparous women or women diagnosed during pregnancy. Here we describe a mouse model of postpartum breast cancer that identifies mammary gland involution as a driving force of tumor progression. In this model, human breast cancer cells exposed to the involuting mammary microenvironment form large tumors characterized by abundant fibrillar collagen, high COX-2 expression, and an invasive phenotype. In culture, tumor cells are invasive in a fibrillar collagen and COX-2-dependent manner. In the involuting mammary gland, inhibition of COX-2 reduces the collagen fibrillogenesis associated with involution, as well as tumor growth and tumor cell infiltration to the lung. These data support further research to determine whether women at high-risk for postpartum breast cancer would benefit from treatment with NSAIDs during postpartum involution.

Corresponding Author: Pepper Schedin, PhD, Division of Medical Oncology, MS8117, RC-1 S, 8401K, 12801 E. 17th Avenue, UCD, Aurora, CO 80045, Phone: 303-724-3873, Fax: 303-724-3889, Pepper.Schedin@UCDenver.edu.
*these authors contributed equally

Completing financial interests: The authors have no competing interests as defined by Nature Publishing Group, or other interests that might be perceived to influence the results and discussion reported in this paper.

Author Contributions: TRL developed the postpartum mouse model, and designed and performed the *in vivo* celecoxib, 2D cell culture, protein expression, 3D collagen, celecoxib, COX-2 knockdown studies, human DCIS studies, and data analyses. JO designed and performed the *in vivo* ibuprofen experiments, collagen Western quantitation, 3D gelatin assay, and data analyses. PJK and MWC performed quantitative SHG collagen imaging and collagen fiber orientation. KE provided critical guidance for the SHG imaging. AM generated GFP expressing MCF10DCIS cells and provided MCF10DCIS cells with stable knockdown of COX-2. ACT performed the human outcome analyses. VB and TRL were responsible for regulatory oversight of human tissue acquisition and VB and PS for human tissue acquisition. PS and VB were responsible for hypothesis development, conceptual design, and all data analysis and interpretation. TRL, JO and PS wrote the manuscript.

Introduction

Lifetime risk for breast cancer is reduced in parous women compared to nulliparous women, provided pregnancy occurs at a relatively young age[1]. However, even with young age at first pregnancy, a transient increased risk for breast cancer is observed with each pregnancy[2]. Importantly, the magnitude and duration of this increased risk is greater in older first time mothers[2]. Given the trend toward delayed childbearing observed in the US and all developing countries[3], breast cancer diagnosed in recently pregnant women is expected to rise[4]. Further, independent of the woman's age and tumor pathologic characteristics, women diagnosed with breast cancer within five years postpartum have an increase in breast cancer related deaths compared to women diagnosed during pregnancy [5–8]. These data indicate that a process subsequent to pregnancy, but not pregnancy per se, contributes to the poor prognosis of postpartum breast cancer.

Decreased survival of women with postpartum breast cancer is often attributed to delayed diagnosis. Although delayed diagnosis is a clinical concern, a biological explanation for the poor prognosis of postpartum breast cancer is its promotion by physiologic attributes unique to the postpartum mammary gland. After lactation, or after parturition in the absence of nursing, the mammary gland undergoes involution. Postpartum involution utilizes coordinated programs of epithelial cell death and stromal remodeling to result in gland architecture that resembles the non-secretory, pre-pregnant state. Evidence shows that the involuting mammary gland displays characteristics similar to wound healing and tumor promotional microenvironments[9–16]. To account for the poor prognosis of postpartum breast cancer, we have proposed that tumor cell exposure to the involuting mammary microenvironment promotes breast cancer metastasis[4,9,13,17].

Collagen deposition is an attribute of wound healing that is evident in the postpartum involuting gland[14] and is emerging as a key player in stromal mediated tumor progression[18,19]. Fibrillar collagen correlates with increased risk for breast cancer, as well as tumor cell proliferation, invasion, and metastasis[18,20,21]. When intestinal epithelial cells are exposed to collagen I, increased cyclooxygenase-2 (COX-2) expression and COX-2 dependent motility are observed[22]. COX-2 is an enzyme that promotes production of prostaglandin mediators of inflammation[23] and COX-2 is a well-established therapeutic target in colon cancer[24–26]. In breast cancer patients, elevated COX-2 expression is observed in ~40% of invasive cases and correlates with poor prognosis[27–3031,32], DCIS recurrence[33], and progression of hyperplasia[34]. In breast cancer outcomes studies, COX-2 inhibition by non-steroidal anti-inflammatory drug (NSAID) use is associated with decreased breast cancer recurrence and related deaths[35,36]. In animal models, COX-2 overexpression induces[37] and knockout reduces [38] mammary tumorigenesis and *in vitro* inhibition of COX-2 reduces breast cancer cell proliferation, migration, and invasion[39]. Finally, in xenografted breast tumor cell populations, high COX-2 expression is associated with infiltration of lung[31], bone[40], and brain[32]. Given the directly proportional relationship observed between collagen and COX-2 in the colon, the presence of increased collagen in the mammary gland during postpartum involution implicates COX-2 as a potential mediator of postpartum breast cancer.

To generate a mouse model of postpartum breast cancer that isolates the tumor promotional effects of involution, we injected human breast tumor MCF10DCIS[41] cells into intact mouse mammary glands that were postpartum and actively involuting (involution group) or quiescent (nulliparous group). Within the mammary gland, MCF10DCIS cells form lesions histologically similar to human ductal carcinoma *in situ* (DCIS) that progress to invasive cancers[41,42]. Here, we demonstrate that progression of MCF10DCIS cells to invasion is

promoted by the involuting mammary microenvironment in a manner that is dependent upon fibrillar collagen and COX-2. Further, we show increased collagen deposition in postpartum involuting breast tissue from women, increased COX-2 protein expression in postpartum DCIS cases, and a correlation between collagen I and COX-2 tumor mRNA expression and disease free survival, implicating this pathway in young women's breast cancer. Based on these observations, we utilized our mouse model to show that treatment with celecoxib and ibuprofen, restricted to the window of postpartum mammary gland involution, reverses the promotional effects of involution on mammary tumor progression.

Results

Involution promotes tumor growth via collagen

Clinically, DCIS lesions are defined by malignant epithelial cells confined within the breast duct by an intact layer of myoepithelial cells, with disruption of the myoepithelial layer indicating progression to invasive carcinoma[43]. To develop a mouse model capable of assessing the impact of postpartum involution on DCIS progression, MCF10DCIS cells were injected into intact mammary glands of immunodeficient (SCID) mice one day post-weaning (involution group) or into mammary glands of age-matched nulliparous mice (nulliparous group). In this model, early DCIS-like lesions were evident as solid clusters of malignant cells separated from the mouse mammary stroma by a continuous layer of human-derived myoepithelium, consistent with previous reports[41],[42]. MCF10DCIS cells formed DCIS lesions that closely resemble clinically relevant subtypes and progression to invasion correlated with loss of the myoepithelial cell layer. Invasive tumors were dominantly triple negative and basal-like[44],[45] (Supplementary Figure 1a–d). At four weeks post-tumor cell injection the involution group mice had a greater than 200% increase in average tumor size (Fig 1a, Supplementary Figure 1e,f). Tumor cell promotion by involution was also observed with two additional cell lines (Supplementary Figure 1e and Schedin Lab, unpublished data). Compared to the nulliparous group, the involution group tumor number (Fig 1b), tumor burden (Fig 1c), and percent Ki67 positive tumor cells (Fig 1d) were also increased, identifying the involuting mammary microenvironment as tumor promotional.

In non-injected SCID mouse mammary glands, we observed increased fibrillar collagen deposition during postpartum involution (Fig 1e&f) and involution group tumors had increased intra-tumor collagen deposition (Fig 1g&h). These data suggest that the collagen-rich microenvironment of the postpartum gland influences collagen deposition within the developing tumor. *In vitro*, tumor cells exposed to collagen I were more proliferative, similar to the involution group tumors (compare Fig 1d to Fig 1i, Supplementary Figure 1g), indicating that elevated deposition of collagen in the involuting mammary gland may contribute to the increased tumor growth observed in involution group mice.

Involution promotes collagen dependent tumor cell dispersion

To determine whether the increased number of tumors observed in the involution group was due to tumor cell dispersion, injected mammary glands were imaged for green fluorescent protein (GFP) labeled MCF10DCIS cells. At three weeks post-injection, a single primary lesion was observed per injected gland in the nulliparous group (Fig 2a, **top panel**), whereas in the involution group additional smaller lesions were observed at sites distant from the primary lesion (Fig 2a, **bottom panel**). To assess the timing of tumor cell dispersion, GFP+ tumor cells were examined at three days post-injection by immunohistochemistry (IHC). Specific to the involution group, tumor cells were detected at high frequency throughout the mammary stroma (Fig 2b, Supplementary Figure 2a) and were present within the mammary vasculature (Fig 2c, **left panel**). Extending these observations, flow cytometry analysis of peripheral blood showed increased circulating GFP+ tumor cells at three days post-tumor

cell injection in the involution group only (Fig 2c, **right panel**, Supplementary Figure 2b), demonstrating tumor cell access to the circulation during involution. Fluorescent *in situ* hybridization (FISH) analysis confirmed MCF10DCIS cell dispersion unique to the involution group within the mammary stroma, mammary vasculature, and mouse lung parenchyma (Fig 2d). To determine whether tumor cell infiltration of the lungs in the involution group was due to the increased size of primary tumors in this group, lung infiltration was quantified from mice with size-matched primary tumors using quantitative reverse transcription polymerase chain reaction (qRT-PCR) for human-specific β2M transcripts. Involution group tumors had higher average human β2M expression in lung tissue compared to the nulliparous group, confirming that the increased invasive potential of involution group tumor cells is independent of tumor size (Fig 2e).

To distinguish whether the involution microenvironment alters the invasive potential of tumor cells in a manner that is maintained ex-vivo, GFP+ tumor cell populations were harvested from involution and nulliparous groups. On average, involution group tumor cell populations were more proliferative (data not shown), and displayed increased motility (Fig 2f) and invasion (Fig 2g) that was collagen I dependent, as all cell populations were non-motile and non-invasive on Matrigel™ (data not shown). Further, the acquisition of motile behavior in the involution group tumor cells on collagen was not dependent on primary tumor size, as tumor cells derived from smaller involution tumors were as motile as tumor cells derived from larger involution tumors (Fig 2h). These data implicate collagen I as a primary mediator of the increased proliferation, motility, and invasion observed in involution group tumors.

Fibrillar collagen and COX-2 drive invasive phenotype

In vivo, high expression of COX-2 was observed in tumor cells adjacent to high-density collagen (Fig 3a, **arrows**), involution group tumors demonstrated overall increased COX-2 expression (Fig 3b), and Western blot analysis of pooled tumor cell lysates confirmed increased COX-2 protein expression in tumor cell populations isolated from involution group tumors (Fig 3c). In an *in vitro* wound closure assay, tumor cell motility was reduced 50%-80% with selective inhibition of COX-2 using the NSAID celecoxib (CXB) (Fig 3d). Evidence that tumor cell interaction with collagen I induces COX-2 was observed in three dimensional (3D) culture where COX-2 expression in MCF10DCIS cells correlated directly with collagen I concentration (Fig 3e, Supplementary Figure 3a). Increasing COX-2 expression also correlated with increased invasive morphology (Fig 3e&f, Supplementary Fig 3b&c) consistent with a role for COX-2 in mediating invasion on collagen. Supporting these observations, both celecoxib and shRNA knockdown of COX-2 decreased tumor cell invasive morphology observed on collagen (Fig 3g&h, Supplementary Fig 3d).

Studies by others suggest that mammary tumor cell invasion and access to the vasculature is gained through migration along collagen fibers[18],[46]. Further, radial alignment of collagen is characteristic of tumor-associated collagen and is implicated in tumor cell invasion[46]. Evaluation of collagen organization during involution revealed that collagen fibers were aligned radially to ducts in the involution group at almost twice the frequency as observed in the nulliparous group (0.94 vs 0.58 radially aligned fibers per duct analyzed)(Fig 3i, **arrow**). Consistent with these data, induction of invasion *in vitro* was dependent upon fibrillar collagen, as denatured collagen (gelatin) was unable to induce tumor cell invasion (Fig 3j). Of note, cells on denatured collagen upregulated COX-2 yet did not invade (Supplementary Fig 3e&f), indicating that invasion is context dependent requiring both fibrillar collagen and COX-2. Our data suggest that the increased deposition of fibrillar collagen during involution directly increases COX-2 expression in tumor cells and further, that tumor cells require COX-2 to migrate along collagen fibers.

In vivo, specific inhibition of COX-2 during postpartum involution resulted in reduction of tumor growth (Fig 4a, Supplementary Fig 4a) and dispersion (Fig 4b&c) consistent with roles for COX-2 in tumor cell proliferation and invasion. Surprisingly, COX-2 inhibition during involuting also decreased mammary gland collagen deposition and frequency of radial fibers to nulliparous amounts (0.81 vs 0.43 fibers per duct analyzed) (Fig 4d&e, Supplementary 4b). These unexpected results suggest that COX-2 inhibitors block collagen fibrillogenesis during postpartum mammary gland involution, as well as directly target tumor cell COX-2 expression that results from interaction with collagen, as modeled in Figure 4f.

Collagen and COX-2 may impact postpartum breast cancer

In order to address whether the collagen and COX-2 pathway may be applicable to postpartum breast cancer in women, collagen deposition and orientation were analyzed in breast tissue of young women. In comparison to breast tissue from nulliparous women, involuting breast tissue showed increased deposition of collagen and more than twice the frequency of radially aligned fibers (0.43 vs 1.0 radially aligned fibers per duct analyzed) (Fig 5a&b, Supplementary Fig 5a&b). Based on these observations and the link between collagen and tumor cell COX-2 expression described above, we examined whether collagen I and COX-2 expression correlates with early relapse in young women with breast cancer. These analyses were restricted to women ≤ 45 based on a previous definition of young women's breast cancer[47] and recent data generated from our Young Women's Breast Cancer Translation Program clinical dataset demonstrating that ~33% of women ≤ 45 with breast cancer are diagnosed within 6 years of giving birth (Borges and Schedin, unpublished observations). Eleven publicly available microarray datasets were analyzed (details in Supplementary Table 1), resulting in a combined dataset consisting of 345 cases ≤ 45 years of age at diagnosis who relapsed within five years. In this data set, high Col1AI1and COX-2 (gene name: prostaglandin-endoperoxide synthase 2, *PTGS2*) expression correlated with decreased relapse free survival with a hazard ration of 1.45, (95% CI: 1.08-1.95, multivariate Cox proportional-hazards model) that was independent of estrogen receptor (ER) status (Fig 5c, Supplementary Fig 5c&d). Importantly, high Col1A1 or COX-2 alone, or any other combination of Col1A1 and COX-2 expression, did not correlate with early relapse in univariate Cox proportional-hazards models (Fig 5d Supplementary Fig 5d), consistent with our *in vitro* data demonstrating a requirement for both fibrillar collagen and COX-2 in driving cellular invasion (Supplementary Fig 3e&f). Further, in the NKI295 dataset, high Col1 and COX-2 positively correlated with an activated wound response-gene expression signature previously shown to associate with decreased metastasis free and overall survival in breast cancer subjects[48] (Supplementary Fig 5e). Finally, in a small independent data set, analysis of DCIS lesions in nulliparous and postpartum women revealed increased COX-2 protein expression in the postpartum DCIS lesions (Fig 5e&f, Supplementary Fig 5f). These correlative results provide impetus for further study into the role of collagen and COX-2 in human postpartum breast cancer.

Ibuprofen suppresses tumor progression during involution

Having identified COX-2 as a potential mediator of postpartum breast cancer we tested whether ibuprofen, a safer NSAID than celecoxib for postpartum women, could decrease tumor promotion in rodents. *In vitro*, ibuprofen blocked motility of the highly invasive involution tumor cell populations by ~80% (Fig 6a). Further, as observed with celecoxib in mice, treatment of rats with ibuprofen during involution reduced mammary gland collagen deposition and frequency of radial fibers to nulliparous amounts (0.98 vs 0.33 radially aligned fibers per duct analyzed) (Fig 6b, Supplementary Fig 6a). To assess efficacy of ibuprofen in the postpartum breast cancer model, involution group mice were treated with ibuprofen or vehicle for 14 days post-weaning (Supplementary Fig 6b). Ibuprofen treatment

did not affect regression of the mammary epithelium that occurs during postpartum involution (Fig 6c) or nulliparous group tumor growth (Fig 6d, Supplementary Fig 6c). However, in involution mice, ibuprofen treatment mitigated the increased tumor growth and COX-2 expression to nulliparous amounts (Fig 6d,e&f, Supplementary Fig 6d,e), as well as reduced tumor cell infiltration of the lung (Fig 6g&h, Supplementary Fig 6f).

Discussion

Given the functional plasticity of the adult mammary gland, breast tumors are exposed to distinct microenvironments that may alter progression and outcome of the disease. Here we investigated the effect of postpartum mammary gland involution on DCIS progression. The process of postpartum involution utilizes aspects of wound healing programs known to be tumor promotional[14–17], which may account for the increased metastasis observed in breast cancers following pregnancy[4–8,17,49–51]. Our studies build on previous work showing that tumors are promoted by postpartum mammary gland involution[9,13,52] and specifically by extracellular matrix proteins isolated from involuting mammary glands[9,13]. We demonstrate a mechanism for involution induced breast tumor progression that involves interaction between fibrillar collagen and COX-2, two established tumor promotional molecules previously unlinked in the breast[18,19,21,31,32,37–40,46,53]. We demonstrate that COX-2 activity within the normal involuting gland is required for deposition of fibrillar collagen and that this collagen upregulates COX-2 in tumor cells. Supportive of this link, normal mouse mammary epithelial cells cultured in high density collagen upregulate COX-2 mRNA ~4 fold[21] and PGE2, a product of COX-2 activity, promotes collagen production during wound healing in skin [54]. Thus, we identify two distinct roles for COX-2 in promotion of breast tumors during involution; COX-2 activity in the host promotes mammary collagen fibrillogenesis and COX-2 activity within the tumor cell promotes invasion.

We also report that collagen associated with physiologically normal postpartum involution has radial alignment, an organization previously observed only in invasive breast tumors[46]. Recently, radial aligned collagen was demonstrated to be an independent poor prognostic indicator in breast cancer[55]. We propose that radial collagen architecture in the involuting gland provides tracks whereby COX-2 expressing tumor cells exit the duct, migrate into surrounding stroma and intravasate, similar to collagen-mediated tumor cell migration observed in other models[18,19,21,46,53]. Surprisingly, COX-2 inhibition by NSAIDs during normal postpartum mammary gland involution blocked production and radial organization of fibrillar collagen. This observation suggests that modulation of collagen fibrillogenesis is a novel mechanism by which NSAIDs exhibit anti-tumor activity.

Importantly, our data compiled from human breast tissues is consistent with the collagen and COX-2 pathway contributing to the poor prognosis of women with postpartum breast cancer. However, validation of these observations in larger cohorts would further test this hypothesis. Nonetheless, observations from our pre-clinical studies showing reduced tumor growth and metastatic potential with ibuprofen and celecoxib suggest that further research into COX-2 inhibitor use might provide a novel strategy to improve the prognosis of young women should they be diagnosed with postpartum breast cancer. Supportive of this strategy, we provide evidence that ibuprofen does not interfere with normal postpartum gland regression. Further, relevance to chemoprevention in recently pregnant women at high risk for breast cancer is evident, as ibuprofen is a safe, affordable, over-the-counter-NSAID and duration of the treatment would be limited. An intriguing question unexplored in our studies is whether an NSAID based chemoprevention strategy can reduce incidence of postpartum breast cancer; an extremely desirable objective given the 6 million pregnancies per year in the US.

Methods

Rodent Breeding

SCID mice (Taconic or Charles River Laboratories) and Sprague-Dawley rats (Taconic) were housed and bred as previously described[14], with age-matched nulliparous animals set aside for controls. Pups were weaned to initiate involution 10–14 d post-parturition. Celecoxib (Pfizer) was delivered at 500 mg kg^{-1} chow as previously described[56] for 14 d starting at weaning. Ibuprofen (Sigma), 360 mg kg^{-1} in irradiated powdered rodent diet (Harlan Tekland) was delivered at 30mg mg kg^{-1} body weight per day for 6 d (rat) or 14 d (mouse) starting at weaning. Rats were sacrificed at 6 d post-weaning. All animal procedures were approved by University of Colorado Institutional Animal Care and Use Committee.

Cell culture

MCF10DCIS.com and shRNA derivatives, a gift from Kornelia Polyak, were cultured as previously described[42]. GFP derivatives were created by transduction with pLVX-AcGFP lentiviral vector (Invitrogen). 3D transwell assays were modified from previously published protocols[57] with details in Supplementary Methods.

Tumor model

200,000 DCIS or DCIS-GFP cells in 50 ul PBS were injected into right and left #4 mammary gland fat pads of involution group mice one day post-weaning or age-matched nulliparous group mice. Mice were sacrificed at 1 and 3 d, or 3, 4, 6, and 8 weeks post-injection for tissue and/or RNA. Each study was replicated 2–3 times. For Figure 2e, qRT-PCR analyses were performed on mice with 2.0 cm^3 primary tumors. Sacrifice for qRT-PCR analyses in Figure 6 was based on the five largest tumors at each timepoint per group. For immunofluorescent images, mice were sacrificed three weeks post-injection and representative images depicted.

Human tissue acquisition

Research utilizing de-identified human breast tissue was conducted under a protocol deemed exempt from subject consent as approved by the Colorado Multiple Institution Review Board (COMIRB) and tissues acquired as previously reported[14].

Fluorescent *In Situ* Hybridization (FISH) analysis

FISH analyses for human and mouse Cot-1 DNA was performed as described[13] by the UCCC Cytogenics Core. Mammary tumor, mouse mammary stroma, and mammary vasculature, were histologically identified in serial sections.

Western blot analysis

Collagen-1 and COX-2 (Cayman Chemical) analyses were performed as described[14].

Tumor cell populations

Tumor cell populations were obtained from mammary tumors 3 weeks post injection and were confirmed to be > 95% GFP+. Wound closure and invasion assays were performed according to published protocols[13,58]. Additional details in Supplementary Methods.

Flow cytometry analysis

0.1 mL of blood was added to 3 mL RBC lysis buffer (eBioscience), incubated at for 15 min, then diluted with 9 ml PBS. Cells were pelleted (300–400x*g*) at 4 °C and resuspended

in 1 ml PBS. GFP+ tumor cell information was collected and analyzed on a Beckman Coulter CyAn ADP© using Summit© software in the UCCC Flow Cytometry Core.

Immunohistochemistry

Lungs and mammary glands (tumors intact) were prepared for H&E, IHC, and Masson's trichrome as described[14]. Antibody information is in Supplemental Table 1. Quantification of total tumor area (necrotic and stromal areas removed) and percent positive stain was performed using Image J and/or Aperio Analysis software with details in Supplementary Methods.

Quantitative RT-PCR

Mouse lung tissue was collected in RNAlater (Qiagen) and homogenized in QIAzol (Qiagen) in Lysing Matrix A tubes on a FastPrep-24 machine (MP Biomedicals). RNA was isolated and purified, 3 μg of RNA was used for cDNA synthesis followed by qRT-PCR analysis as described[13]. Calculation and normalization details are described in supplementary methods.

Multiphoton Second Harmonic Generation (SHG) microscopy

Five μm unstained tissue sections were imaged at the University of Wisconsin Laboratory for Optical and Computational Instrumentation as described[21,46]. Details are provided in supplementary methods.

Analyses of clinical outcome and gene expression data

Gene expression and clinical outcome data of 2,685 breast cancer subjects was obtained from eleven public data sets (Details in Supplementary Methods and Table 1). We assessed *PTGS2* (COX2) and COL1A1 expressions in subjects age ≤ 45 who relapsed within 5 years of diagnosis in each data set and divided them into high or low expression for each gene (above or below mean expression in each dataset). We grouped the subjects into high COX2 and high COL1A1 and other combinations of COX2 and COL1A1 expressions. Univariate and multivariate of Cox proportional-hazards regressions on ER status, COX2 expression, COL1A1 expression, and the combination of COX2 and COL1A1 on 345 subjects were performed using MedCalc Statistical Software. χ^2 test was used to correlate COX2 and COL1A1 expressions with the wound healing gene expression signature for the NKI-295 data set. $P < 0.05$ was considered statistically significant.

Statistical analyses of pre-clinical studies

Unpaired t and ANOVA (across all conditions) tests were performed using GraphPad InStat software, assuming independent samples and normal distributions. Advanced analyses were performed by the UCD School of Public Health Biostatistics and Informatics Research Consulting Laboratory, with details described in the Supplementary Methods.

Supplementary Material

Refer to Web version on PubMed Central for supplementary material.

Acknowledgments

We are grateful to K. Polyak (Harvard Medical School) and lab member M. Hu for providing MCF10DCIS parental cells and advice, C. Ambrosone (Roswell Park Cancer Institute), L. Hines (University of Colorado, Colorado Springs), A. Thor and Susan Edgerton of the University of Colorado Denver for human tissue acquisition, M. Garcia and M. Skokan of the University of Colorado Cancer Center Cytogenics Core for FISH analysis, M. Lucia and R. Wilson for assistance with quantitative IHC analysis, O. Maller, K. Bell, S. Jindal, K. Hedman, D. Powell,

N. DeWaele, and Y. Kwarteng for technical assistance, and S. Sillau for advanced statistical analyses. We thank K. Polyak, A. Thorburn, and M. Moss and *Nature Medicine* Reviewers for critical evaluation of the manuscript, and we gratefully acknowledge the patients for their contribution to this research.

Grant Support: Supported by Department of Defense Synergistic Idea Award #BC060531, Komen Foundation #KG090629, Mary Kay Ash Foundation #078-08 and University of Colorado Cancer Center grants to PS and VB, Department of Defense Award #BC074970 to PJK, American Cancer Society New England Division Postdoctoral Fellowship Spin Odyssey #PF-08-257-01-CSM to TRL, Department of Defense Postdoctoral grant BC087579 to AM, and Department of Defense Predoctoral Grant #BC073482 to JO.

Abbreviations

3D	three dimensional
COX-2	cyclooxygenase-2
DCIS	ductal carcinoma in situ
ER	Estrogen receptor
FISH	fluorescent in situ hybridization
GFP	green fluorescent protein
IHC	immunohistochemistry
NSAID	non-steroidal anti-inflammatory drug
PTGS2	prostaglandin-endoperoxide synthase 2, gene name for COX-2
qRT-PCR	quantitative reverse transcription polymerase chain reaction
SCID	severe combined immune deficiency
SHG	second harmonic generation

References

1. Lord SJ, et al. Breast cancer risk and hormone receptor status in older women by parity, age of first birth, and breastfeeding: a case-control study. Cancer Epidemiol Biomarkers Prev. 2008; 17:1723–1730. [PubMed: 18628424]
2. Lambe M, et al. Transient increase in the risk of breast cancer after giving birth. The New England journal of medicine. 1994; 331:5–9. [PubMed: 8202106]
3. Mathews, TJ.; Hamilton, BE. Delayed Childbearing: More Women Are Having Their First Child Later in Life. Vol. Vol. 21. Hyattsville, MD: National Center for Health Statistics; 2009.
4. Lyons TR, Schedin PJ, Borges VF. Pregnancy and breast cancer: when they collide. Journal of mammary gland biology and neoplasia. 2009; 14:87–98. [PubMed: 19381788]
5. Daling JR, Malone KE, Doody DR, Anderson BO, Porter PL. The relation of reproductive factors to mortality from breast cancer. Cancer Epidemiol Biomarkers Prev. 2002; 11:235–241. [PubMed: 11895871]
6. Whiteman MK, et al. Reproductive history and mortality after breast cancer diagnosis. Obstet Gynecol. 2004; 104:146–154. [PubMed: 15229014]
7. Dodds L, et al. Relationship of time since childbirth and other pregnancy factors to premenopausal breast cancer prognosis. Obstet Gynecol. 2008; 111:1167–1173. [PubMed: 18448751]
8. Stensheim H, Moller B, van Dijk T, Fossa SD. Cause-specific survival for women diagnosed with cancer during pregnancy or lactation: a registry-based cohort study. J Clin Oncol. 2009; 27:45–51. [PubMed: 19029418]
9. Bemis LT, Schedin P. Reproductive state of rat mammary gland stroma modulates human breast cancer cell migration and invasion. Cancer research. 2000; 60:3414–3418. [PubMed: 10910049]
10. Schedin P, Mitrenga T, McDaniel S, Kaeck M. Mammary ECM composition and function are altered by reproductive state. Molecular carcinogenesis. 2004; 41:207–220. [PubMed: 15468292]

11. Clarkson RW, Wayland MT, Lee J, Freeman T, Watson CJ. Gene expression profiling of mammary gland development reveals putative roles for death receptors and immune mediators in post-lactational regression. Breast Cancer Res. 2004; 6:R92–R109. [PubMed: 14979921]
12. Stein T, et al. Involution of the mouse mammary gland is associated with an immune cascade and an acute-phase response, involving LBP, CD14 and STAT3. Breast Cancer Res. 2004; 6:R75–R91. [PubMed: 14979920]
13. McDaniel SM, et al. Remodeling of the mammary microenvironment after lactation promotes breast tumor cell metastasis. The American journal of pathology. 2006; 168:608–620. [PubMed: 16436674]
14. O'Brien J, et al. Alternatively activated macrophages and collagen remodeling characterize the postpartum involuting mammary gland across species. The American journal of pathology. 2010; 176:1241–1255. [PubMed: 20110414]
15. Schafer M, Werner S. Cancer as an overhealing wound: an old hypothesis revisited. Nat Rev Mol Cell Biol. 2008; 9:628–638. [PubMed: 18628784]
16. Coussens LM, Werb Z. Inflammation and cancer. Nature. 2002; 420:860–867. [PubMed: 12490959]
17. Schedin P. Pregnancy-associated breast cancer and metastasis. Nature reviews. 2006; 6:281–291.
18. Wang W, et al. Single Cell Behavior in Metastatic Primary Mammary Tumors Correlated with Gene Expression Patterns Revealed by Molecular Profiling. Cancer research. 2002; 62:6278–6288. [PubMed: 12414658]
19. Butcher DT, Alliston T, Weaver VM. A tense situation: forcing tumour progression. Nature reviews. 2009; 9:108–122.
20. Paszek MJ, et al. Tensional homeostasis and the malignant phenotype. Cancer cell. 2005; 8:241–254. [PubMed: 16169468]
21. Provenzano PP, et al. Collagen density promotes mammary tumor initiation and progression. BMC medicine. 2008; 6:11. [PubMed: 18442412]
22. Broom OJ, Massoumi R, Sjolander A. Alpha2beta1 integrin signalling enhances cyclooxygenase-2 expression in intestinal epithelial cells. J Cell Physiol. 2006; 209:950–958. [PubMed: 16972245]
23. Mann JR, Backlund MG, DuBois RN. Mechanisms of disease: Inflammatory mediators and cancer prevention. Nat Clin Pract Oncol. 2005; 2:202–210. [PubMed: 16264935]
24. Thun MJ, Namboodiri MM, Heath CW Jr. Aspirin use and reduced risk of fatal colon cancer. The New England journal of medicine. 1991; 325:1593–1596. [PubMed: 1669840]
25. Elder DJ, Paraskeva C. COX-2 inhibitors for colorectal cancer. Nat Med. 1998; 4:392–393. [PubMed: 9546780]
26. Sheehan KM, et al. The relationship between cyclooxygenase-2 expression and colorectal cancer. Jama. 1999; 282:1254–1257. [PubMed: 10517428]
27. Ristimaki A, et al. Prognostic significance of elevated cyclooxygenase-2 expression in breast cancer. Cancer research. 2002; 62:632–635. [PubMed: 11830510]
28. Denkert C, et al. Elevated expression of cyclooxygenase-2 is a negative prognostic factor for disease free survival and overall survival in patients with breast carcinoma. Cancer. 2003; 97:2978–2987. [PubMed: 12784332]
29. Spizzo G, et al. Correlation of COX-2 and Ep-CAM overexpression in human invasive breast cancer and its impact on survival. British journal of cancer. 2003; 88:574–578. [PubMed: 12592372]
30. Howe LR. Inflammation and breast cancer. Cyclooxygenase/prostaglandin signaling and breast cancer. Breast Cancer Res. 2007; 9:210. [PubMed: 17640394]
31. Minn AJ, et al. Genes that mediate breast cancer metastasis to lung. Nature. 2005; 436:518–524. [PubMed: 16049480]
32. Bos PD, et al. Genes that mediate breast cancer metastasis to the brain. Nature. 2009; 459:1005–1009. [PubMed: 19421193]
33. Gauthier ML, et al. Abrogated response to cellular stress identifies DCIS associated with subsequent tumor events and defines basal-like breast tumors. Cancer cell. 2007; 12:479–491. [PubMed: 17996651]

34. Visscher DW, et al. Association between cyclooxygenase-2 expression in atypical hyperplasia and risk of breast cancer. Journal of the National Cancer Institute. 2008; 100:421–427. [PubMed: 18334709]
35. Kwan ML, Habel LA, Slattery ML, Caan B. NSAIDs and breast cancer recurrence in a prospective cohort study. Cancer Causes Control. 2007; 18:613–620. [PubMed: 17404892]
36. Holmes MD, et al. Aspirin intake and survival after breast cancer. J Clin Oncol. 2010; 28:1467–1472. [PubMed: 20159825]
37. Liu CH, et al. Overexpression of cyclooxygenase-2 is sufficient to induce tumorigenesis in transgenic mice. The Journal of biological chemistry. 2001; 276:18563–18569. [PubMed: 11278747]
38. Howe LR, et al. HER2/neu-induced mammary tumorigenesis and angiogenesis are reduced in cyclooxygenase-2 knockout mice. Cancer research. 2005; 65:10113–10119. [PubMed: 16267038]
39. Larkins TL, Nowell M, Singh S, Sanford GL. Inhibition of cyclooxygenase-2 decreases breast cancer cell motility, invasion and matrix metalloproteinase expression. BMC cancer. 2006; 6:181. [PubMed: 16831226]
40. Singh B, et al. COX-2 involvement in breast cancer metastasis to bone. Oncogene. 2007; 26:3789–3796. [PubMed: 17213821]
41. Miller FR, Santner SJ, Tait L, Dawson PJ. MCF10DCIS.com xenograft model of human comedo ductal carcinoma in situ. Journal of the National Cancer Institute. 2000; 92:1185–1186. [PubMed: 10904098]
42. Hu M, et al. Regulation of in situ to invasive breast carcinoma transition. Cancer cell. 2008; 13:394–406. [PubMed: 18455123]
43. Allred DC, et al. Ductal carcinoma in situ and the emergence of diversity during breast cancer evolution. Clin Cancer Res. 2008; 14:370–378. [PubMed: 18223211]
44. Sorlie T, et al. Gene expression patterns of breast carcinomas distinguish tumor subclasses with clinical implications. Proceedings of the National Academy of Sciences of the United States of America. 2001; 98:10869–10874. [PubMed: 11553815]
45. van de Vijver MJ, et al. A gene-expression signature as a predictor of survival in breast cancer. The New England journal of medicine. 2002; 347:1999–2009. [PubMed: 12490681]
46. Provenzano PP, et al. Collagen reorganization at the tumor-stromal interface facilitates local invasion. BMC medicine. 2006; 4:38. [PubMed: 17190588]
47. Anders CK, et al. Breast carcinomas arising at a young age: unique biology or a surrogate for aggressive intrinsic subtypes? J Clin Oncol. 29:e18–e20. [PubMed: 21115855]
48. Chang HY, et al. Robustness, scalability, and integration of a wound-response gene expression signature in predicting breast cancer survival. Proceedings of the National Academy of Sciences of the United States of America. 2005; 102:3738–3743. [PubMed: 15701700]
49. Rodriguez AO, et al. Evidence of poorer survival in pregnancy-associated breast cancer. Obstet Gynecol. 2008; 112:71–78. [PubMed: 18591310]
50. Lethaby AE, O'Neill MA, Mason BH, Holdaway IM, Harvey VJ. Overall survival from breast cancer in women pregnant or lactating at or after diagnosis. Auckland Breast Cancer Study Group. International journal of cancer. 1996; 67:751–755.
51. Bladstrom A, Anderson H, Olsson H. Worse survival in breast cancer among women with recent childbirth: results from a Swedish population-based register study. Clinical breast cancer. 2003; 4:280–285. [PubMed: 14651773]
52. Gupta PB, et al. Systemic stromal effects of estrogen promote the growth of estrogen receptor-negative cancers. Cancer research. 2007; 67:2062–2071. [PubMed: 17332335]
53. Levental KR, et al. Matrix crosslinking forces tumor progression by enhancing integrin signaling. Cell. 2009; 139:891–906. [PubMed: 19931152]
54. Wilgus TA, et al. The impact of cyclooxygenase-2 mediated inflammation on scarless fetal wound healing. The American journal of pathology. 2004; 165:753–761. [PubMed: 15331400]
55. Conklin MW, et al. Aligned collagen is a prognostic signature for survival in human breast carcinoma. The American journal of pathology. 178:1221–1232. [PubMed: 21356373]

56. Howe LR, et al. Celecoxib, a selective cyclooxygenase 2 inhibitor, protects against human epidermal growth factor receptor 2 (HER-2)/neu-induced breast cancer. Cancer research. 2002; 62:5405–5407. [PubMed: 12359744]

57. Krause S, Maffini MV, Soto AM, Sonnenschein C. A novel 3D in vitro culture model to study stromal-epithelial interactions in the mammary gland. Tissue engineering. 2008; 14:261–271. [PubMed: 18694322]

58. Liang CC, Park AY, Guan JL. In vitro scratch assay: a convenient and inexpensive method for analysis of cell migration in vitro. Nature protocols. 2007; 2:329–333.

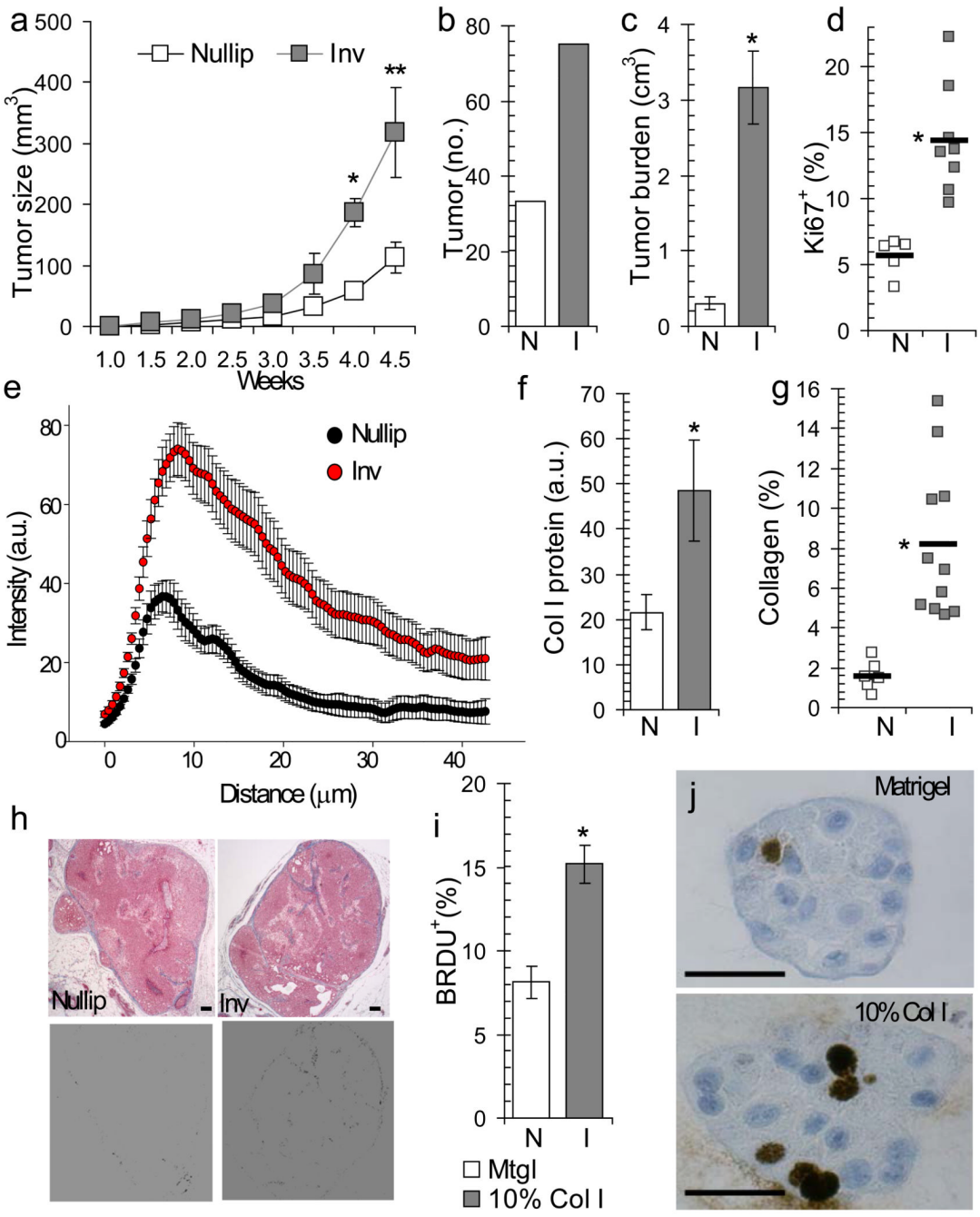

Figure 1. Postpartum mammary microenvironment promotes tumor growth in a mammary fat pad xenograft model

(**a**) Average primary tumor volume, **p*=0.001, ***p*=0.0174, *n*=7 (nulliparous), *n*=6 (involution), unpaired t test. (**b**) Total tumor number per group at 4 weeks post-injection, *n*=9 (nulliparous) and *n*=8 (involution). (**c**) Average tumor burden (total tumor volume per injected gland) 4 weeks post-injection, **p*=0.0011, *n*=15 (nulliparous), *n*=13 (involution), unpaired t test. (**d**) Average percent tumor area positive for Ki67, **p*=0.0009, *n*=5 (nulliparous), *n*=8 (involution), unpaired t test. (**e**) Collagen intensity measured by Second Harmonic Generation (SHG) imaging versus distance from involuting mouse mammary ducts (red, *n*=17 ducts, 3 mice) compared to nulliparous (black, *n*=12 ducts, 3 mice),

p<0.00001, student's t test. (**f**) Western blot for Collagen I in mouse mammary tissue lysates, *p=0.042, n=3 per group, unpaired t test. (**g**) Percent tumor area positive for collagen by trichrome stain, *p=0.0002, n=6 (nulliparous), n=11 (involution), unpaired t test. (**h**) Top, trichrome stained tumor images, blue=collagen. Bottom, blue signal converted to black, scalebar=100 μm. (**i**) Percent BRDU+ cells in 3D culture on Matrigel or 10% collagen I, *p<0.0001, unpaired t test, n=30 100X fields per group. (**j**) BRDU IHC images of 3D organoids, scalebar=50 μm. N=nullip=nulliparous (white), I=inv=involution (gray), data are presented as mean +/− SEM.

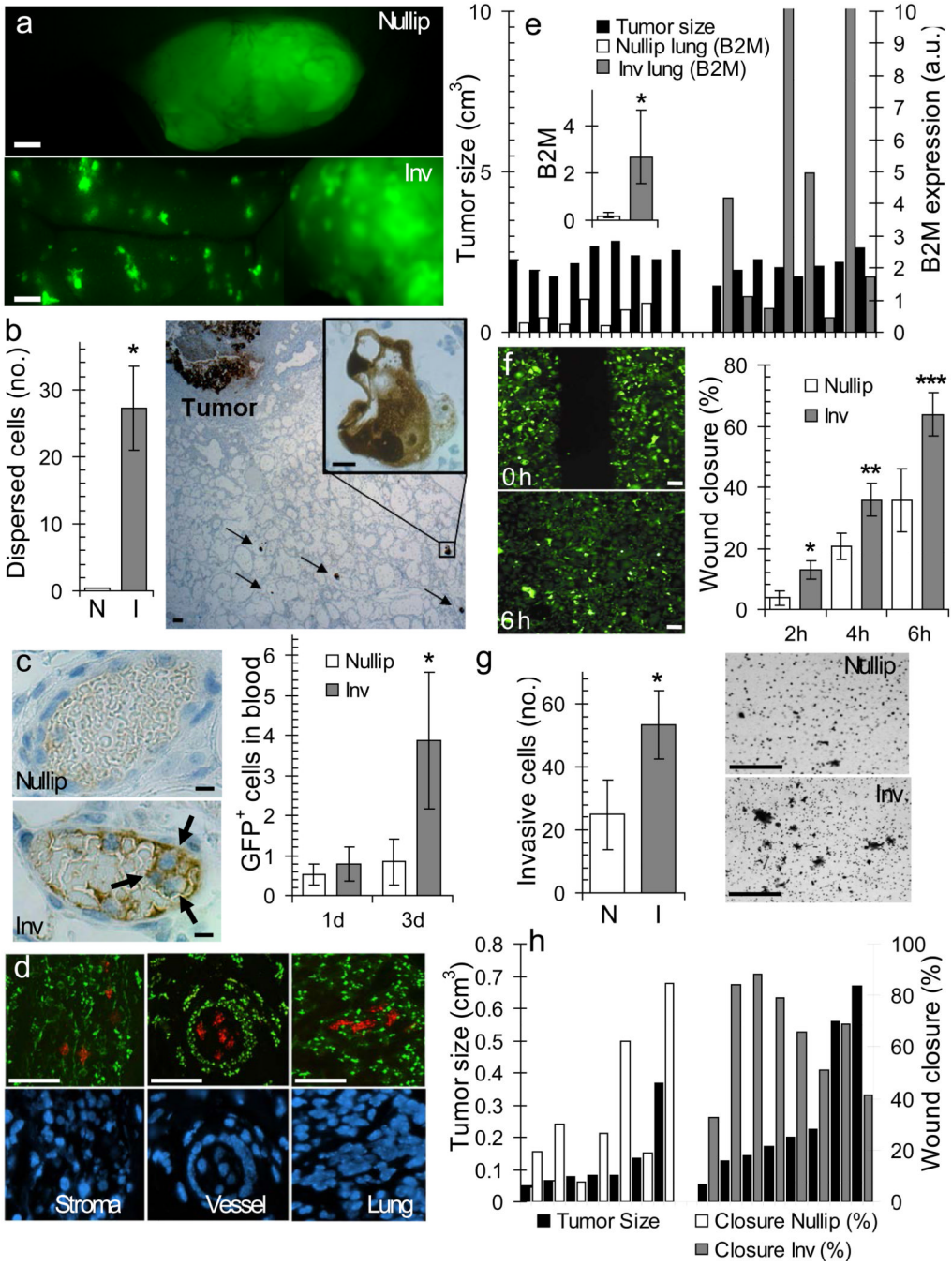

Figure 2. Postpartum involution drives tumor cell invasion

(**a**) GFP+ tumor cells 3 weeks post injection, scalebar=100 μm. (**b**) IHC image of GFP+ cells in mammary tissue 3 d post-injection, scalebar=50 μm, inset GFP+ tumor cells, scalebar=10 μm, and quantification of dispersed GFP+ cell clusters by group, **p*=0.0129, *n*=3 (nulliparous), *n*=5 (involution), unpaired t test. (**c**) IHC image of tumor cells in mammary blood vessel 3 d post-injection, scalebar=10 μm. Quantification of tumor cells in peripheral blood 1 and 3 d post-injection, **p*=0.04, *n*=3 per group, unpaired t. (**d**) Fluorescent *in situ* hybridization for COT-1 DNA (human=red, mouse=green) and DAPI-stained nuclei (blue), scalebar=50 μm. (**e**) Left axis, individual mammary tumor volumes

(black bars). Right axis, qRT-PCR analysis of lung for human β2M transcripts in arbitrary units (a.u.) after normalizing to actin. Inset, average β2M expression **p*=0.0046, *n*=9 (nulliparous #1-9), *n*=8 (involution #10-17), unpaired t test. (**f**) Right, average *in vitro* wound closure of Involution and Nulliparous Group tumor cell populations on collagen 2, 4, and 6 h post-scrape **p*=0.034, ***p*=0.045, ****p*=0.040, *n*=7 (nulliparous), *n*=8 (involution). Left, scrape images of Involution Group tumor cell populations at 0 h and 6 h (scalebar=50 μm). (**g**) Left, average number of invasive tumor cells in transwell assay, *n*=5 (nulliparous), *n*=6 (involution), **p*=0.0491 unpaired t-test. Right, filter images, scalebar=50 μm. (**h**) Left axis, volumes of tumors utilized for tumor cell isolation (black bars). Right axis, wound closure of individual tumor cell populations 6h post-scrape. N=nullip=nulliparous (white), I=inv=involution (gray), data are mean +/− SEM.

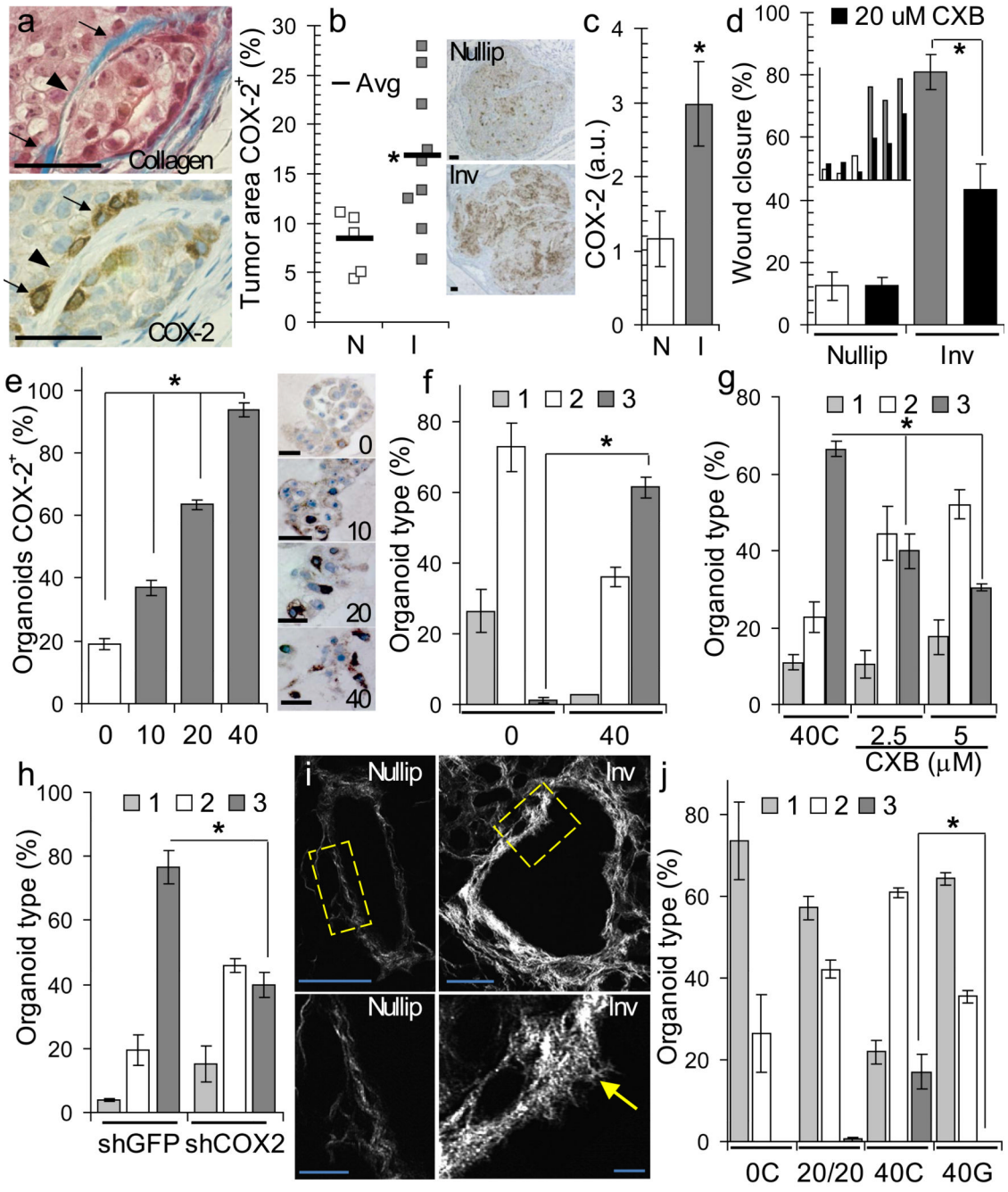

Figure 3. Fibrillar collagen and COX-2 mediate tumor cell invasiveness

(**a**) Trichrome (top) and COX-2 (bottom) IHC-stained tumor, arrows=dense collagen, arrowhead=sparse collagen, scalebar=50 μm. (**b**) Right, percent tumor COX-2+ by IHC, **p*=0.0275, *n*=9 (nulliparous), *n*=5 (involution), unpaired t test Left, COX-2 IHC images, scalebar=100 μm. (**c**) Western blot showing expression of COX-2 in tumor cell populations, **p*=0.0274, *n*=3 per group, unpaired t test. (**d**) *In vitro* wound closure by tumor cells on collagen +/− 20 μM COX-2 inhibitor celecoxib (CXB, black) at 6h post-scrape, **p*=0.019, *n*=3 cell populations per group, unpaired t test. Inset: individual tumor cell population data. (**e**) Left, % COX-2+ organoids by IHC in Matrigel™ or Matrigel™ + 10% (10), 20% (20),

and 40% (40) collagen, *p<0.0001, one-way ANOVA. Right, 3D-organoid COX-2 IHC images, scalebar=50 μm. (**f,g,h**) % organoids rounded(1), dysmorphic(2), or invasive(3) on (**f**) 0 and 40% collagen, *p<0.0001, *n*=3 wells per condition, one way ANOVA, (**g**) on 40C + DMSO solvent, 40C + 2.5 μm CXB, 40C + 5 μm CXB, *p<0.0001, *n*=3 wells per condition, one way ANOVA and (**h**) on 40C + shGFP and 40C + shCOX-2, *p<0.0001, *n*=3 wells per condition, one way ANOVA. (**i**) Left, SHG image of collagen surrounding nulliparous and involuting ducts, higher magnifications (yellow box) below, scalebar=10 μm. Arrow: radially aligned collagen, scalebar=50 μm. (**j**) Organoid type on 0C, 20% collagen + 20% gelatin (20/20), 40C and 40% gelatin (40G), *p<0.0001, *n*=3 wells per condition, one way ANOVA. Data are mean +/− SEM and representative of triplicate studies.

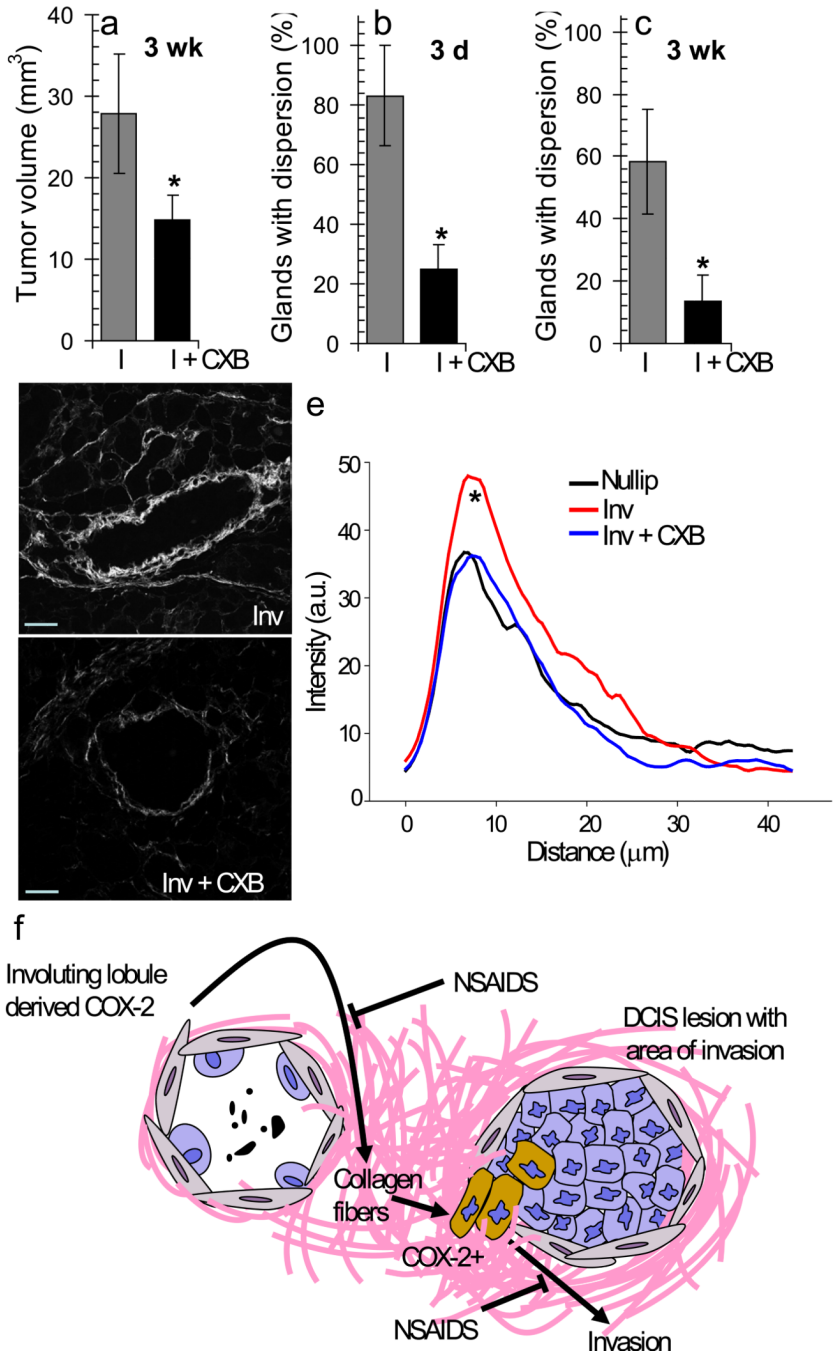

Figure 4. COX-2 inhibition mitigates the tumor promotional effects of involution

(**a**) Average tumor volume for involution group (I) and involution+CXB group (I + CXB) mice at 3 weeks post-injection, p=0.0205, n=12, unpaired t test. (**b**) % glands with dispersed GFP+ tumor cells in mammary glands at 3 d post-injection, p=0.018, n=12, unpaired t test. (**c**) % glands with dispersed GFP+ tumor cells in mammary glands at 3 weeks post-injection, p=0.0033, n=12, unpaired t test. Data are presented as mean +/− SEM. (**d**) SHG imaging of collagen surrounding control involuting (Inv)and CXB treated involuting ducts (Inv + CXB), scalebar=50 μm. (**e**) Collagen intensity by SHG versus distance from involuting mouse mammary ducts (red, n=21 ducts, 3 mice) compared to involuting + CXB (green,

n=22 ducts, 3 mice) and to nulliparous (black, *n*=12 ducts, 3 mice), p<0.001 Involution vs Involution + CXB between 5–10 um, student's t test. (f)A model depicting COX-2, derived from the involuting mammary gland, mediated upregulation of collagen fibrillogenesis and subsequent upregulation of COX-2 and invasion (brown cells) in tumor cells exposed to involution collagen.

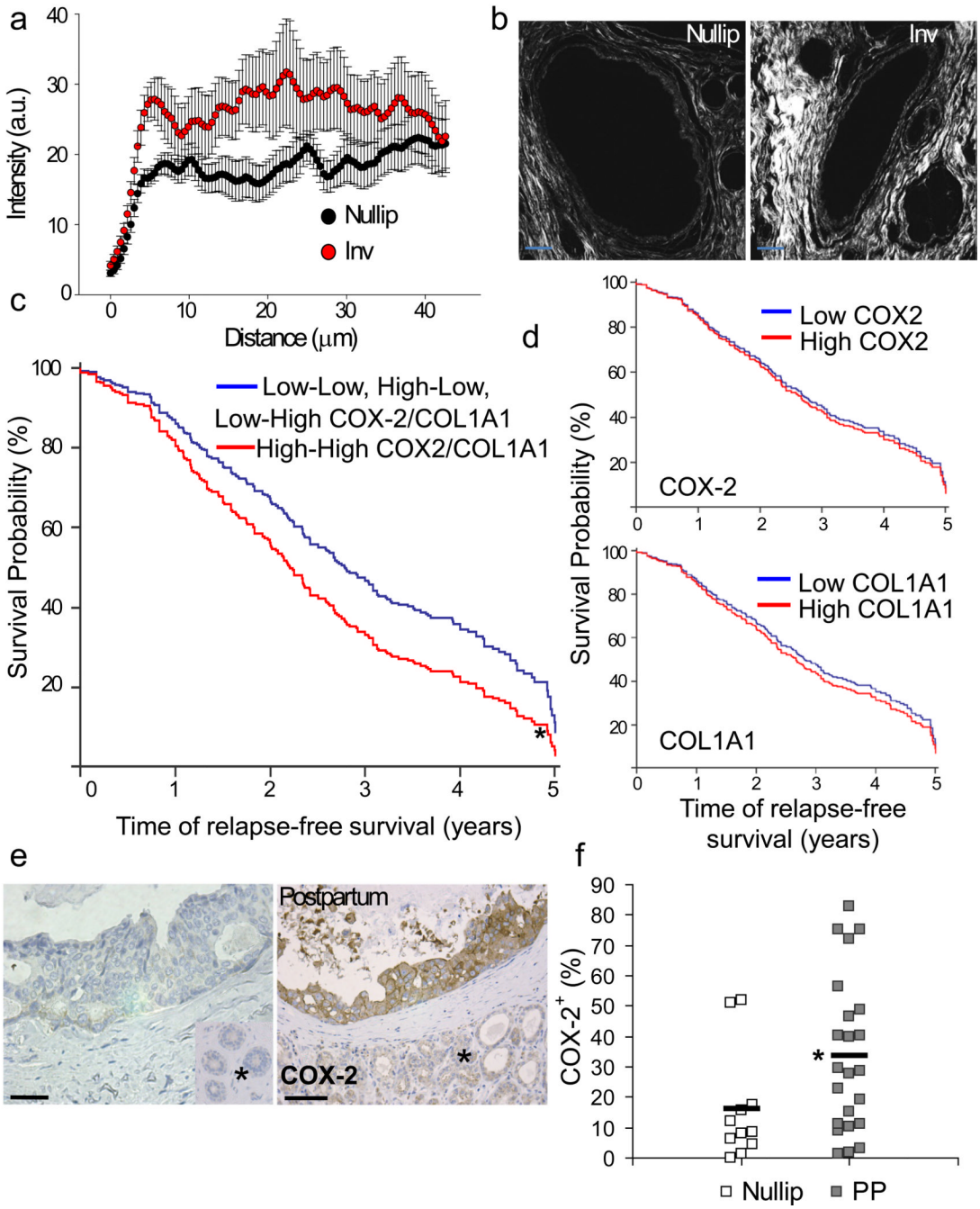

Figure 5. Evidence for collagen and COX-2 contributing to postpartum breast cancer

(**a**) Quantification of collagen intensity by SHG versus distance from human breast ducts, black=nulliparous, red=involution (13–14 ducts per case, 3 cases per group), p<0.00001, student's t test. Data are presented as mean +/− SEM. (**b**) SHG imaging of collagen in breast tissue from involuting (inv) and nulliparous (nullip) women, scalebar=50 μm. (**c**) Multivariate Cox Analysis of relapse free survival in 345 breast tumors diagnosed in women ≤45 years of age who relapsed within five years of diagnosis for effect of high Col1A1 and COX-2 (gene name: *PTGS2*) expression (23%) (1-red dashed line), all other combinations of Col1A1 and COX-2 expression (77%) (0-blue line), and ER status (58% pos and 42% neg).

High Col1A1 and COX-2 is the only significant variable p=0.018. Univariate analysis of (**d**) high COX-2 and (**e**) high COL1A1 and relapse free survival in 345 breast tumors diagnosed in women ≤45 years of age who relapsed within five years of diagnosis. (**f**) Left, images of human DCIS lesions stained for COX-2 by IHC, scalebar=50 μm, * normal adjacent tissue. (**g**) percent area positive for COX-2 signal quantitated by quantitative IHC methods[14], p= 0.0266 n=11 nulliparous cases and 22 cases diagnosed ≤ 10 yrs postpartum (2–13 DCIS lesions examined per case), unpaired t-test. See Supplementary Fig 4c for data set characteristics. Nullip=nulliparous (white), PP=postpartum (gray), black bars indicate group average.

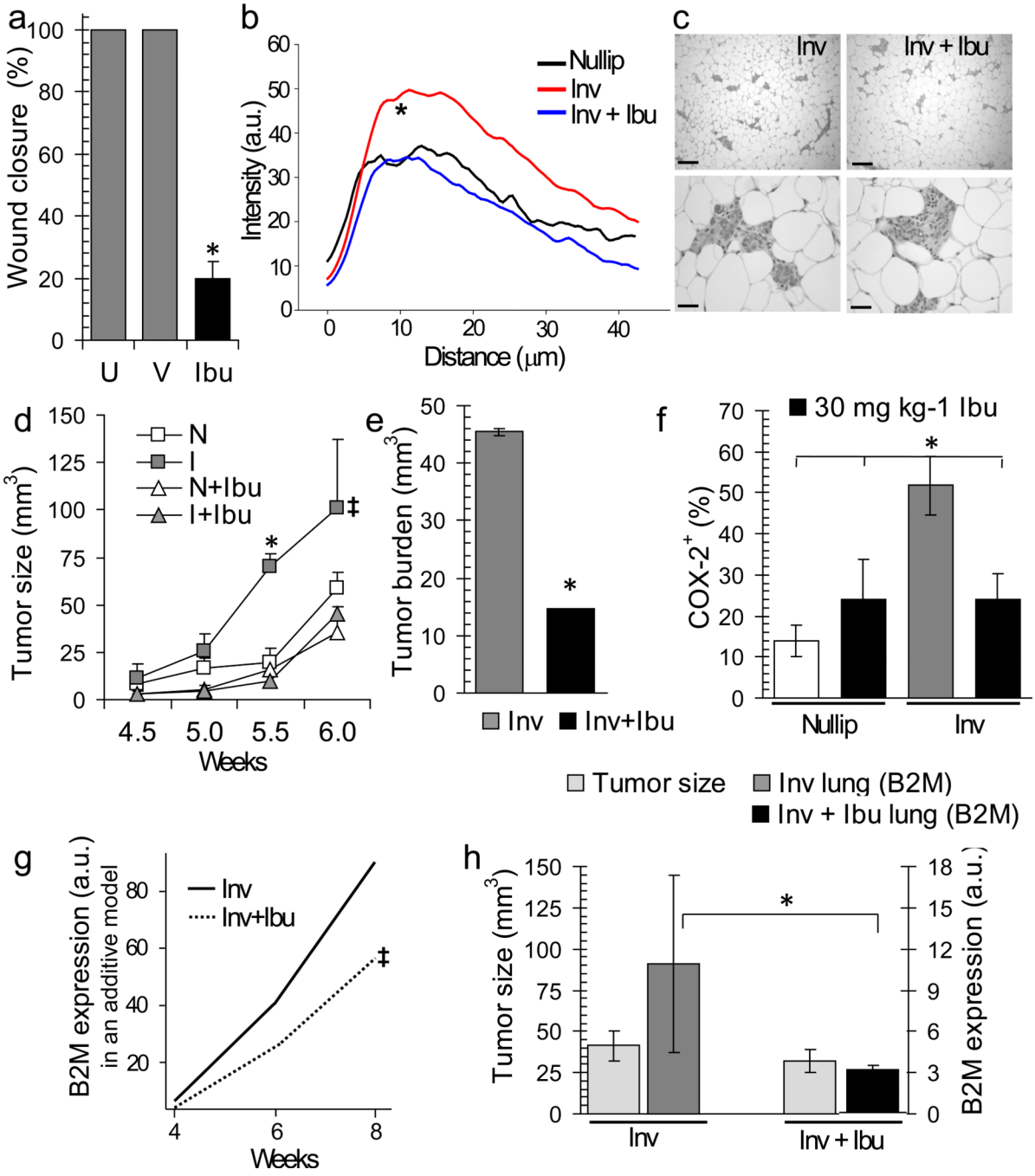

Figure 6. Postpartum ibuprofen treatment reduces tumor volume, burden, COX-2, and lung infiltration

(**a**) *In vitro* wound closure untreated (U), vehicle treated (V), and ibuprofen treated (200μg mL^{-1}) (Ibu), **p*=0.0001, *n*=4 wells per condition, unpaired t test. (**b**) Collagen quantification by SHG as intensity versus distance from rat mammary ducts, black=nulliparous, red=involution, green = involution + ibuprofen (3 rats per Group) p<0.001, involution v involution+ibuprofen between 5–10 um from duct, student's t test. (**c**) H&E images of involution and involution+ibuprofen group mouse mammary tissues 2 weeks post-treatment, top scalebars=150 μm, bottom scalebars=40 μm. (**d**) Average tumor volume in nulliparous (N), involution (I), +/− ibuprofen (Ibu) group mice, **p*=0.00373, one way ANOVA,

‡p≤0.035, type IIIF test for group effect in additive model, *n*=6 (nulliparous), *n*=8 (involution), *n*=4 (nulliparous + ibuprofen), *n*=5 (involution + ibuprofen). (**e**) Tumor burden, 6 week timepoint, **p*=0.0255, *n*=8 (involution), *n*=9 (involution+ibuprofen), unpaired t test. (**f**) Quantitation of tumor COX-2 expression at 6 week timepoint, *p≤0.036, unpaired t test, *n*=9 (nulliparous), *n*=9 (involution), *n*=6 (nulliparous+ibuprofen), *n*=9 (involution +ibuprofen). (**g**) Statistical modeling of mouse lung signal for human-specific β2M by qRT-PCR across time, ‡*p*=0.027, t test of group effect. (**h**) Left axis, average mammary tumor volume per Group demonstrating size-match between groups, (light gray). Right axis, mouse lung signal for human-specific β2M by qRT-PCR analysis, **p*=0.011, *n*=5, Wilcoxon test, involution=dark gray, involution+ibuprofen=black. Data are mean +/− SEM.